



**HAL**  
open science

# Surface Effects Leading to Unusual Size Dependence of the Thermal Hysteresis Behavior in Spin-Crossover Nanoparticles

Jorge Linares, Catalin Jureschi, Kamel Boukheddaden

► **To cite this version:**

Jorge Linares, Catalin Jureschi, Kamel Boukheddaden. Surface Effects Leading to Unusual Size Dependence of the Thermal Hysteresis Behavior in Spin-Crossover Nanoparticles. *Magnetochemistry*, 2016, 2 (2), pp.24. 10.3390/magnetochemistry2020024 . hal-03047965

**HAL Id: hal-03047965**

**<https://hal.science/hal-03047965>**

Submitted on 7 Jun 2023

**HAL** is a multi-disciplinary open access archive for the deposit and dissemination of scientific research documents, whether they are published or not. The documents may come from teaching and research institutions in France or abroad, or from public or private research centers.

L'archive ouverte pluridisciplinaire **HAL**, est destinée au dépôt et à la diffusion de documents scientifiques de niveau recherche, publiés ou non, émanant des établissements d'enseignement et de recherche français ou étrangers, des laboratoires publics ou privés.



Distributed under a Creative Commons Attribution 4.0 International License

Article

# Surface Effects Leading to Unusual Size Dependence of the Thermal Hysteresis Behavior in Spin-Crossover Nanoparticles

Jorge Linares <sup>1,\*</sup>, Catalin Maricel Jureschi <sup>2,3</sup> and Kamel Boukheddaden <sup>1,\*</sup>

<sup>1</sup> GEMAC, Université de Versailles Saint-Quentin-CNRS, Université Paris Saclay, 45 avenue des Etats-Unis, Versailles 78035, France

<sup>2</sup> LISV, Université de Versailles Saint-Quentin-en-Yvelines, Université Paris Saclay, Velizy 78140, France; catalin.jureschi@gmail.com

<sup>3</sup> Faculty of Electrical Engineering and Computer Science and MANSiD, Stefan cel Mare University, Suceava 720229, Romania

\* Correspondence: jorge.linares@uvsq.fr (J.L.); kamel.boukheddaden@uvsq.fr (K.B.); Tel.: +33-139-254-661 (J.L.); +33-139-254-664 (K.B.)

Academic Editor: Guillem Aromí

Received: 22 January 2016; Accepted: 11 April 2016; Published: 3 May 2016

**Abstract:** We analyze the size effect on spin-crossover transition nanoparticles in a 2D Ising-like model subject to a specific ligand-field at the surface. By anisotropic sampling method applied to the finite 2D square Ising lattices with various sizes, we determined the density of macro states by scanning the spin configurations. This information, which is independent on the system parameters, is used to exactly calculate the thermal behavior of spin-crossover nanoparticles whose ligand-field of the atoms at the surface is lower than those of the bulk. We found that decreasing the size of the nanoparticles leads to a global increase of the effective interaction, which has the consequence to enhance the width of the thermal hysteresis. This unusual behavior opens a new avenue in controlling the bistability characteristics at small scale, one of the important conditions of applicability of these materials at the nanometric scale.

**Keywords:** spin crossover; phase transition; nanoparticles; surfaces effects; Monte Carlo simulations

## 1. Introduction

In recent years, there has been a growing interest in the field of spin-crossover (SCO) solids. Under various constraints, such as temperature [1] or pressure [2–4] variations, irradiation by visible light [5–9] or magnetic fields [10], SCO solids can be switched from a low-spin (LS) state to a high-spin (HS) state, and conversely [11,12]. For example, Fe(II) SCO compounds [13] are diamagnetic ( $S = 0$ , LS) and paramagnetic ( $S = 2$ , HS) in the low- and high-temperature phases, respectively. The spin-crossover transition involves both electronic transformation (spin and orbital), and structural modifications. In the case of Fe(II) compounds the metal-ligand bond lengths change by about 0.2 Å, (~10%) and the ligand-metal-ligand bond angles by 0.5°–8° [6,14]. Optical properties are also changed [5,15,16], with usually a colorless HS state and a strongly-colored LS state. Consequently, magnetic and optical measurements [17–21] are the major experimental techniques used for quantitative investigations of the spin transitions. In many cases, elastic interactions between the SCO units are strong enough to induce hysteresis at the thermal spin transition [22] which occurs as a first-order phase transition. Such “switchable” molecular solids are promising in terms of optical data storage [23].

For a few years, the synthesis and the design of spin-crossover nanoparticles have become possible and several interesting behaviors have been reported [24–35]. The experimental results, for most of these studies, confirmed the expected narrowing of the hysteresis loop and, in some cases, the collapse

of the loop below some “critical size”, but very few of them provided a coherent set of data over the relevant size range, that is, above and below the critical size. In addition, the samples usually present a rather wide distribution of sizes, various shapes, and particles were often aggregated in various manners. All of these features obviously impact the switching behavior of the SCO nanoparticles and made the investigation on the properties of a unique nanoparticle a very challenging goal. From the theoretical point of view, there were a few studies of the thermal and photo-switching properties of SCO nanoparticles [36–39], which aimed at reproducing the collapse of the hysteresis effects at the critical size of the particles. These theoretical studies were based on Metropolis simulations on finite size lattices with free boundary conditions. Here, we introduce an additional aspect, which is the specific electronic state of the atoms located at the surface of the nanoparticle. This was suggested by a recent experimental investigation [26], on SCO nano-particles of Fe(pyrazine)[Pt(CN)<sub>4</sub>], with well-controlled sizes above and below the critical size. In addition to the expected narrowing of the hysteresis loop upon decreasing size, this system displayed a sizable lowering of the transition temperature and an increase of the residual HS fraction. The latter features are explained by the different coordination of the surface atoms, including water molecules instead of the organic ligands. These SCO surface atoms experience a weaker ligand-field capable of trapping them in the HS state, which consequently lowers the equilibrium temperature of the particle through a negative pressure effect. For practical reasons the present investigation was performed on 2-D networks where this specific effect was located at the edges. It will be consequently referred to in terms of “edge effect”. Although the present 2-D model might be considered as a preliminary approach to future 3-D models, it is also relevant due to the particular geometry of the nano-crystals which are in shape of square platelets with a rather constant thickness. The core of the square lattice is already submitted to a quasi-uniform effect from both surfaces, irrespective of the size of the network, and the size effect effectively reduces to a 2-D problem. This viewpoint will be supported by the present simulations. We performed Monte Carlo (MC) simulations using the well-known Ising-like Hamiltonian (interacting two-level systems), widely used in literature to describe the equilibrium [40,41] and non-equilibrium [42] properties of SCO solids. This choice was dictated by the simplicity of this description, despite of its phenomenological character. The paper is organized as follows: Section 2 is devoted to the model; Section 3 to the results and their discussion; Section 4 is dedicated to a detailed comparison to experimental data, including the impact of size distributions, and Section 5, to our conclusion.

## 2. Results

In order to reproduce first-order phase transition in 1D-SCO, Linares *et al.* [43] have introduced a short- and a long-range interaction to the Ising-like model [40,41]. Later on, and in order to take into account the matrix effect, Chiruta *et al.* [44] have added an additional interaction term which accounts for the SCO molecules at the surface with the environment (matrix effect), this is termed, the matrix interaction  $L$ .

Thus, the system’s Hamiltonian can be written as follows:

$$H = \frac{\Delta - k_B T \ln g}{2} \sum_{i=1}^{N_t} \sigma_i - J \sum_{\langle i,j \rangle} \sigma_i \sigma_j - G \langle \sigma \rangle \sum_{i=1}^{N_t} \sigma_i - L \sum_{i=1}^{N_s} \sigma_i \quad (1)$$

In Equation (1), the HS and LS states are associated, respectively, with the eigenvalues +1 and –1 of the fictitious spin operator,  $\sigma$ , with their respective different degeneracies  $g_+$  and  $g_-$ , the ratio of which, is denoted,  $g = \frac{g_+}{g_-}$ . These degeneracies account for both internal (spin, orbit, and intermolecular vibrations) and external (lattice phonons) degrees of freedom. Here,  $\Delta$  is the energy difference  $E(\text{HS}) - E(\text{LS})$  between the spin states of isolated molecules, and  $J$  is the coupling parameter accounting for short-range ferroelastic interactions between spin states, here limited to first-neighboring molecules; and  $G$  is the long-range part of the interaction, which is identified as due to lattice phonons and volume change accompanying the transition. The energetic contribution  $L$  ( $>0$ ), limited to surface atoms,

describes the additional “negative” ligand-field felt by the surface atoms. This contribution may arise from coordinated water molecules which substitute to one or several nitrogen atoms linked to the Fe center, or may also be due to the elastic effect of the surrounding polymeric matrix (with bigger lattice parameter than that of the embedded SCO nanoparticle). Let us denote by,  $N_t = N_x^2$ , the total number of atoms, by  $N_c = (N_x - 2)^2$  the number of atoms in the bulk or the core, and by  $N_s = 4(N_x - 1)$ , the number of atoms at the “surface” (edges),  $N_x \times N_x$  square lattice.

Hamiltonian Equation (1) can be re-expressed as a function of the dimensionless macroscopic variables,  $m$ ,  $s$  and  $c$ , given by:

$$m = \sum_{i=1}^{N_t} \sigma_i \quad (2)$$

$$s = \sum_{\langle i,j \rangle} \sigma_i \sigma_j \quad (3)$$

and:

$$c = \sum_{i=1}^{N_s} \sigma_i \quad (4)$$

which are, respectively, associated with the total fictitious magnetization, two spin correlations, and the surface fictitious magnetization. Within these parameters, the total Hamiltonian of Equation (1) is re-written as:

$$H = \left( \frac{\Delta - k_B T \ln g}{2} - G \langle \sigma \rangle \right) m - Js - Lc \quad (5)$$

The associated bulk and surface order parameters of the system, denoted here  $m_V$  and  $m_s$ , are then simply defined as:

$$m_V = \langle \sigma_V \rangle = \frac{\sum_{i=1}^{N_t} \sigma_i}{N_t} \quad (6)$$

and:

$$m_s = \langle \sigma_s \rangle = \frac{\sum_{i=1}^{N_s} \sigma_i}{N_t} \quad (7)$$

The HS fractions,  $n_s$  (surface), and  $n_V$  (volume), connect to these two quantities through the general relation:

$$n_i = \frac{1 + m_i}{2} \quad (i = s, v) \quad (8)$$

The equilibrium temperature  $T_{eq}$  is defined as the temperature for which the average spin value  $\langle \sigma \rangle$  is equal to zero ( $m_V = 0$ ), which leads to a HS fraction equal to 1/2. The present model involves two local situations, the features of which are listed in Table 1. The key point is that the specific weaker effective ligand fields ( $\Delta - 2L$ ) at the surface act as a negative (but non uniform) pressure on the system through the interaction of surface atoms with their nearest neighboring bulky atoms. As a matter of fact, these contributions should be included in the total ligand-field.

**Table 1.** The ligand field as function of the molecules' positions in the lattice.

Description	Total	Edges	Core
Number of atoms	$N_x^2$	$4(N_x - 1)$	$(N_x - 2)^2$
Ligand-field	-	$\frac{\Delta - 2L - k_B T \ln g}{2}$	$\frac{\Delta - k_B T \ln g}{2}$

Hamiltonian Equation (1) was exactly solved in the canonical approach. The parameter values were chosen from typical data in spin-crossover literature, such as the molar entropy change  $\Delta S \approx 50$  J/K/mol leading to  $\ln(g) = \Delta S/R \approx 6.01$  (where  $R$  is the gas constant) and energy gap  $\Delta/k_B = 1300$  K leading to a typical value of the equilibrium temperature  $T_{eq} = \Delta/(k_B \ln(g)) \approx 216.3$  K. The short-range interaction parameter,  $J$ , is taken equal to  $J/k_B = 15$  K and the long-range parameter,  $G$ , is taken equal to  $G/k_B = 172.7$  K. The interaction between the edge molecules and the environment,  $L$ , is taken equal to  $L/k_B = 120$  K.

The exact calculations were performed on square lattices of size  $N_x \times N_x$  up to  $N_x = 12$ , using open boundary conditions in order to fairly take into account for the experimental situation of SCO nanoparticles having a specific ligand field at the surface. Next, the thermal dependence of the HS fraction,  $n_{HS}(T)$ , for several lattice sizes were determined. The results are summarized in Figure 1. The system was warmed from  $T = 175$  K to 225 K and cooled down to the initial temperature 175 K by 1 K steps. The total HS fraction,  $n_{HS}(T)$ , was obtained from Equation (8) where:

$$m = \langle \sigma \rangle = \frac{\sum_{i=1,NL} \frac{m_i}{N} d(m_i s_i c_i) \exp\left(-\frac{1}{k_B T}(-h_f m_i - J s_i - L c_i)\right)}{\sum_{i=1,NL} d(m_i s_i c_i) \exp\left(-\frac{1}{k_B T}(-h_f m_i - J s_i - L c_i)\right)} \quad (9)$$

and  $d(m,s,c)$  is the number of configurations for a given set of values, calculated using Monte Carlo Entropic Sampling (MCES) method, described in the next section.  $NL$  is the number of distinct configurations of states  $m, s, c$  ( $m, s$ , and  $c$  defined by the Equations (2)–(4)) where the “field”  $h_f$  has the expression:

$$h_f = -\left(\frac{\Delta - k_B T \ln g}{2} - G \langle \sigma \rangle\right) \quad (10)$$

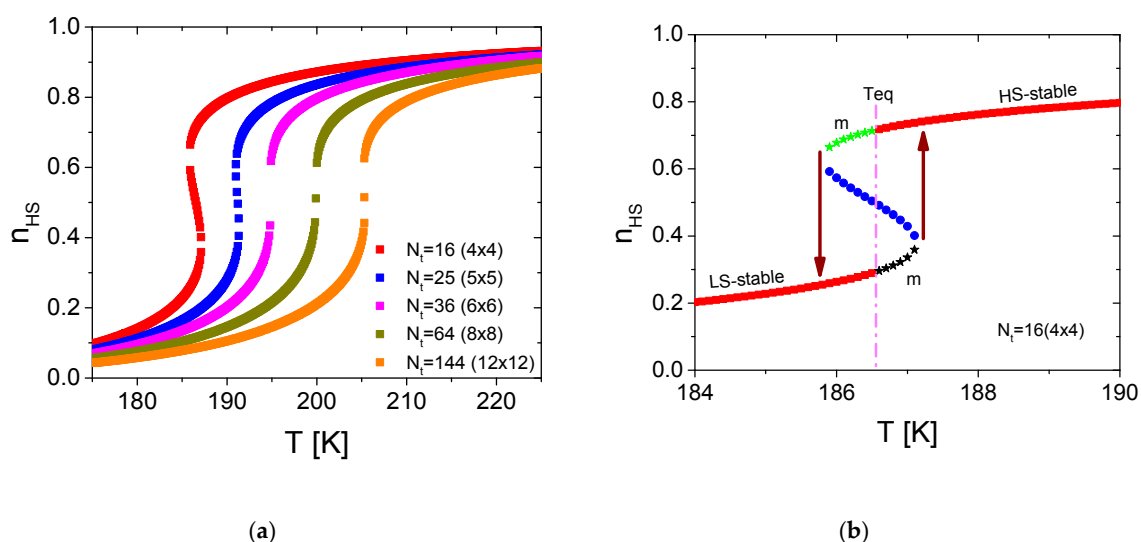


**Figure 1.** (a) The simulated thermal behavior of the total high-spin (HS) fraction,  $n_{HS}(T)$ , for different system sizes, showing an increase of the thermal hysteresis width for smaller nanoparticle sizes; (b) Enlarged view of the simulated thermal behavior of the total HS fraction,  $n_{HS}(T)$ , for  $N_t = 16(4 \times 4)$  molecules, showing the stable (red square), metastable:  $m$  (black and green stars) and unstable (blue dots) regions: only the stable and metastable states are observed at thermal equilibrium. The computational parameters are:  $\Delta/k_B = 1300$  K,  $G/k_B = 172.7$  K,  $J/k_B = 15$  K,  $L/k_B = 120$  K,  $\ln(g) = 6.01$ .

Similarly, the average of the edge molecules is given by the following equation:

$$\langle c \rangle = \frac{\sum_{i=1,NL} \frac{c_i}{N_c} d(m_i s_i c_i) \exp\left(-\frac{1}{k_B T}(-h_f m_i - J s_i - L c_i)\right)}{\sum_{i=1,NL} d(m_i s_i c_i) \exp\left(-\frac{1}{k_B T}(-h_f m_i - J s_i - L c_i)\right)} \quad (11)$$

### 3. Monte Carlo Entropic Sampling

We used the Monte Carlo entropic sampling method [45,46] to generate the table that contains the dimensionless macroscopic variables,  $m$ ,  $s$ ,  $c$ , and their density,  $d(m,s,c)$ . Therefore, we used the principle of MCES described by Shteto *et al.* [45] which consists in introducing in the detailed balance equation of the MC procedure, a suited biased distribution  $P$  in order to favor configurations belonging to weakly degenerate macrostates and to dampen those belonging to the highly degenerate macrostates.

The balance equation is given by:

$$P_i W(i \rightarrow j) = P_j W(j \rightarrow i) \quad (12)$$

and the biasing probability was chosen as the inverse of the desired restricted density of states.

$$P_i \propto \frac{1}{d(m,s,c)} \quad (13)$$

In this case, the balance equation can be written:

$$\frac{W(i \rightarrow j)}{W(j \rightarrow i)} = \frac{P_j}{P_i} = \frac{d(m_i, s_i, c_i)}{d(m_j, s_j, c_j)} \quad (14)$$

Since, in the first Monte Carlo step, the density of the state  $d(m,s,c)$  is unknown we put all  $d(m,s,c)$  equal to 1. So, after iteration  $i$  the density will be  $d_i(m,s,c)$ . Then, using  $d_i(m,s,c)$  as a bias, a MC sampling is run; it is termed a "Monte Carlo stage" and yields a histogram of the frequency of the macrostates [46],  $H_i(m,s,c)$ :

$$H_i(m,s,c) \propto d(m,s,c) \frac{1}{d_i(m,s,c)} \quad (15)$$

The resulting restricted density of states is obtained after was applied the correction for the bias:

$$d_{i+1}(m,s,c) \propto d_i(m,s,c) H_i(m,s,c) \quad (16)$$

After the table that consist from  $m$ ,  $s$ ,  $c$ , and  $d(m,s,c)$  is obtained, the exact partition function can be calculated using the following expression:

$$Z = \sum_{(m,s,c)} d(m,s,c) \exp(-\beta(-hm - Js - Lc)) \quad (17)$$

and so all the thermodynamic properties of the systems can be derived analytically.

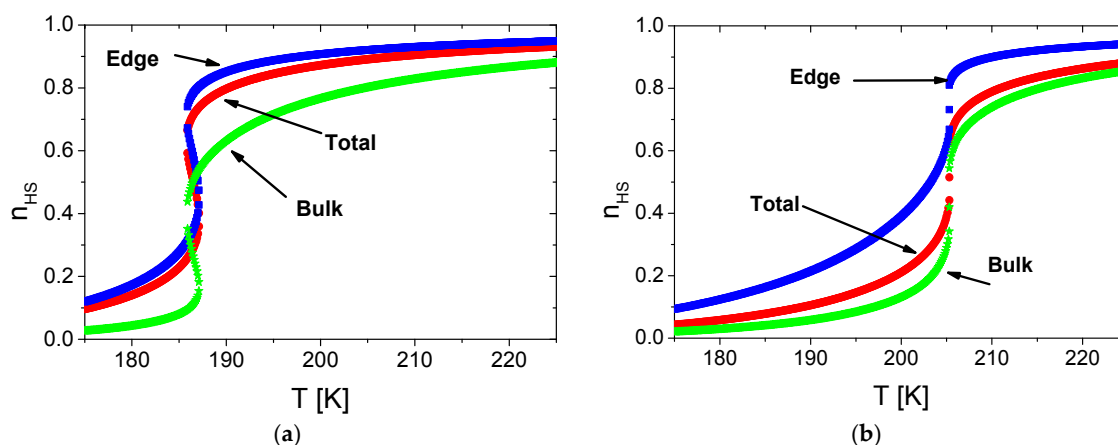
### 4. Results and Discussion

Figure 1 illustrates the thermal behavior of the HS fraction,  $n_{HS}(T)$ , calculated for various particle sizes. Upon decreasing particle size ( $N_x \times N_x$ ) the transition temperature is downward shifted and the width of the thermal hysteresis loop progressively increases as a result of surface effects.

The detailed discussion of the results of the model follows. This behavior contrasts with the classical behavior of the thermal hysteresis with particle size, where indeed it monotonously vanishes at small sizes. To help the reader in identifying the stability of all solutions drawn in the thermal hysteresis, we highlighted in Figure 1b, the stable, metastable and unstable states accompanying the thermally-induced first-order spin-crossover transition. The stable and metastable states are easily identified: HS (LS) is stable for all temperatures bigger (lower) than  $T_{eq}$  and becomes metastable for  $T < T_{eq}$  ( $T > T_{eq}$ ). For all of these branches, increasing the temperature results in the increase of the HS fraction: that is a normal behavior. However, in the middle region of the thermal hysteresis (blue dots in Figure 1b), the HS fraction becomes a decreasing function with temperature ( $\frac{\partial n_{HS}}{\partial T} < 0$ ) which

obviously corresponds to an instability. The situation is somehow similar to the mechanical instability region of a van der Waals gas, where the volume increases under a positively applied pressure.

We could separate the contributions of surface atoms and core atoms in the thermal behavior of the total HS fraction of Figure 1. Figure 2 displays two chosen cases of nanoparticles with sizes  $(4 \times 4)$  and  $(12 \times 12)$  depicting all contributions. One can clearly see, that in both cases, the surface (blue curves) starts to transform much earlier than the core (green curves), which clearly indicates that the surface is driving the thermal LS to HS transitions. It is however obvious that for very bigger sizes (unreachable with MCES method), the contribution of the surface will be marginal and the core will dominate. This tendency is already visible in the case of  $12 \times 12$  particle, in which we remark that the curve of the total response (red) is much more close to that of the bulky atoms.



**Figure 2.** The thermal behavior for the edge, inner and total molecules of the system for the cases: (a)  $N_t = 16$  ( $4 \times 4$ ) and (b)  $N_t = 144$  ( $12 \times 12$ ). The model parameters are the same as those of Figure 1.

#### 4.1. Size Dependence of the Equilibrium Temperature

We found that the size dependence of the transition temperature could be described by analytical laws (easily extended to 3D models). Here, it worth mentioning that even for small sizes, exact analytical solutions of Hamiltonian Equation (1) in 2D are out of reach [47], contrary to our previous studied case where the surface atoms were fixed in the HS state [48].

We introduce here a simple idea that the transition temperature of the system is still the result of a null total effective ligand-field. Taking advantage of the data listed in Table 1, the transition temperature,  $T_{eq}$ , for a square lattice  $N_x \times N_x$  is the solution of the following equation:

$$\frac{\Delta - k_B T_{eq} \ln g}{2} \times (N_x - 2)^2 + \frac{\Delta - 2L - k_B T_{eq} \ln g}{2} \times 4(N_x - 1) = 0 \quad (18)$$

which expresses that the total ligand-field is equal to zero at  $T = T_{eq}$ .

Solving Equation (18) gives the analytical expression of the lattice size-dependence of the transition temperature, as:

$$T_{eq} = \frac{N_c}{N_t} T_{eq}^{bulk} + \frac{N_s}{N_t} T_{eq}^{surf}, \quad (19)$$

which can be written as:

$$N_x^2 T_{eq} = (N_x - 2)^2 T_{eq}^{bulk} + 4(N_x - 1) T_{eq}^{surf}, \quad (20)$$

leading to a parabolic and linear contribution of the bulk and surface contribution to  $N_x^2 T_{eq}$ . These tendencies have been checked numerically in the simulations, and shown in Figure 3, which indicates that from the phenomenological view point, they are followed.



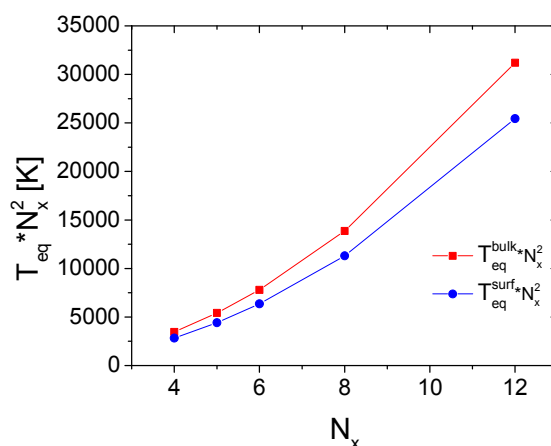


**Figure 3.** The size-dependence of  $N_x^2 T_{eq}$  showing a parabolic behavior for the bulk contribution and a quasi-linear trend for that of the surface, in qualitative good agreement with analytical predictions of Equation (20).

Where  $T_{eq}^{bulk}$  and  $T_{eq}^{surf}$  are the transition temperatures of the bulk and the surface, whose expressions are:

$$T_{eq}^{bulk} = \frac{\Delta}{k_B \ln g} \approx 216.3K \text{ and } T_{eq}^{surf} = \frac{\Delta - 2L}{k_B \ln g} \approx 176.3K \tag{21}$$

Equation (19) predicts that the transition temperature has two limiting values, namely  $T_{eq} = T_{eq}^{surf} = 173.6$  for  $N_x = 2$  for the smallest nanoparticle size, and  $T_{eq} = \frac{\Delta}{k_B \ln g} \approx 216K$  corresponding to the bulk transition temperature, reached for an infinite lattice ( $N_x \rightarrow \infty$ ).

The relevance of Equation (19) is supported by the comparison to the exact results derived from entropic sampling method. As shown in Figure 4, where the global  $T_{eq}$  is plotted vs  $1/N_x$ , the analytical prediction (blue dots) given by Equation (19) is in excellent agreement with the data arising from the simulation (red squares).

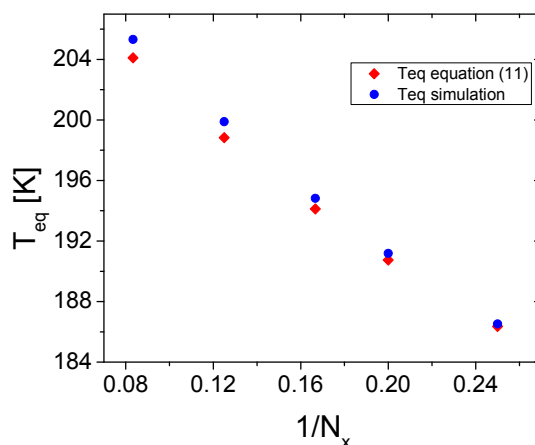


**Figure 4.** Size dependence of the global transition temperature showing an excellent agreement between MC (Monte Carlo) simulations (blue circles) and analytical predictions (red squares) of Equation (19). The computational parameters were:  $\Delta/k_B = 1300$  K,  $G/k_B = 172.7$  K,  $J/k_B = 15$  K,  $L/k_B = 120$  K,  $\ln(g) = 6.01$ .

We should mention that the present model involves the assumption that the effective degeneracy  $g$  is constant. Thus,  $g$  is assumed as independent on the strain at the surface and as well it does not depend on the particle size.



#### 4.2. The Size Dependence of the Hysteresis Loop and the Occurrence of the First-Order Transition

To understand the size effects on the thermal behavior of the HS fraction, we performed MC simulations using the set of parameters given in Figure 1, for which the studied system presents a gradual transition for the biggest studied size (*i.e.*,  $N_x = 12$ ). For that, the short-range interaction parameter was set to  $J/k_B = 15$  K. It is worth mentioning that in the usual Ising-like model, the first-order phase transition takes place only when the condition  $T_{O.D.} > T_{eq}$  is satisfied. Here,  $T_{O.D.}$  is the order-disorder (or Curie) temperature of the corresponding pure Ising model, obtained from Hamiltonian of Equation (1) by putting  $\Delta/k_B = 0$ ,  $L/k_B = 0$  and  $g = 1$  ( $\ln(g) = 0$ ). For  $J = 0$  values, the interactions between SCO sites are of pure long-range nature and so  $T_{O.D.} = G/k_B \sim 172.7$  K (minimum value). For a large lattice size, the equilibrium temperature is dominated by the contribution of the bulk material and leads here to  $T_{eq} \sim T_{eq}^{bulk} \sim 216$  K, which is larger than  $T_{OD}$ , which allows to say that for infinite lattice, the thermal behavior of the HS fraction is that of a gradual conversion. When  $J \neq 0$ , the analytical expression of  $T_{OD}$  is out of reach. So, to determine  $T_{OD}$  for different lattice sizes, we performed MC simulations for  $\Delta/k_B = 0$  K,  $G/k_B = 172.7$  K,  $J/k_B = 15$  K,  $L/k_B = 0$  K, and  $\ln(g) = 0$ . The results are summarized in Figure 5, which shows a net increase of  $T_{OD}$  with the system size, following a simple power law,  $T_{OD} \sim \sqrt{N_x - 4}$ , as demonstrated in Figure 5c.

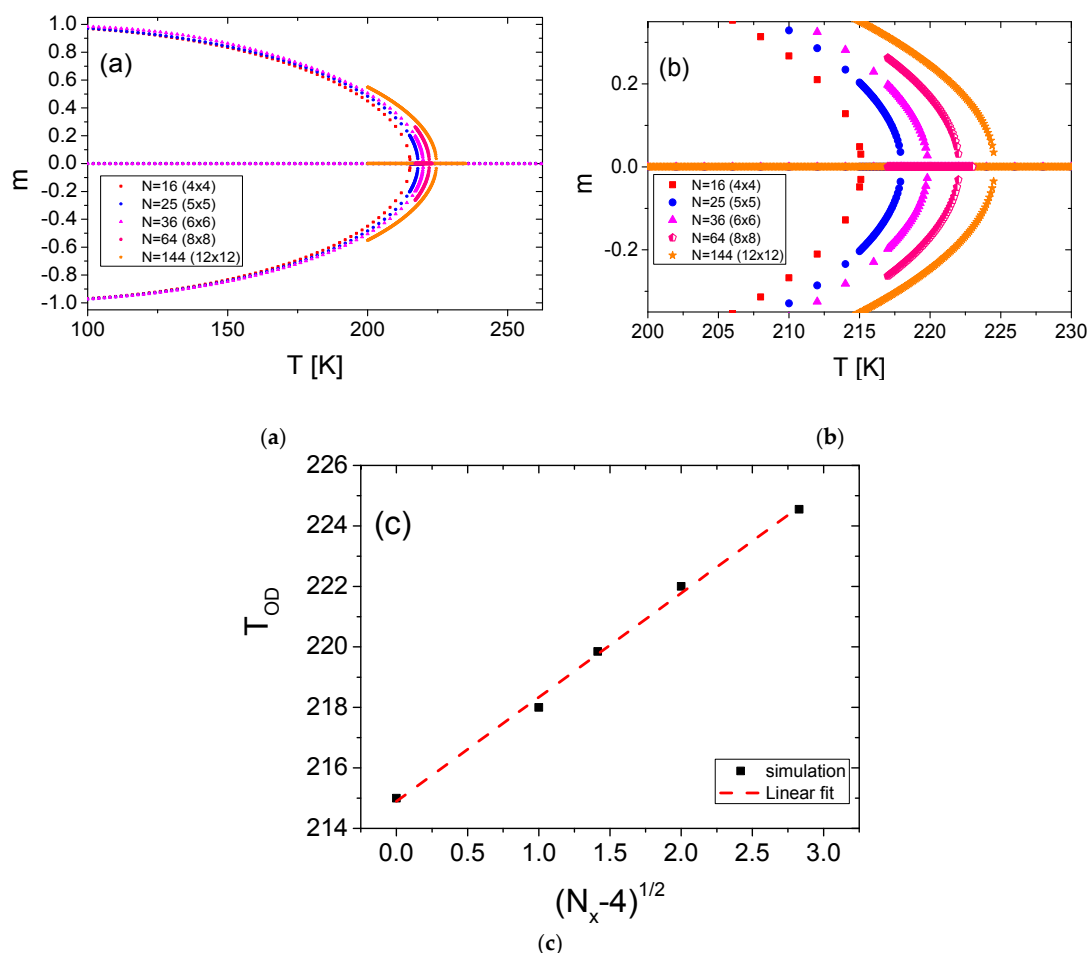


**Figure 5.** (a) The order-disorder temperature,  $T_{O.D.}$ , calculated for different system sizes; (b) zoom around the critical temperatures, showing the increase of  $T_{O.D.}$  with size; and (c)  $T_{OD}$  versus  $\sqrt{N_x - 4}$  showing a linear behavior. The red dashed line is the best linear fit. The computational parameters are:  $\Delta/k_B = 0$  K,  $G/k_B = 172.7$  K,  $J/k_B = 15$  K,  $L/k_B = 0$  K,  $\ln(g) = 0$ .

The values of  $T_{OD}$  vary here from  $\sim 215$  K for a  $4 \times 4$  lattice to  $\sim 224$  K for a  $12 \times 12$  lattice. On the other hand, we found from Figure 1, that  $T_{eq} \sim 204$  K ( $< T_{O,D} = 224$ ) for the lattice  $12 \times 12$ . Consequently, according to the simple criteria of the simple Ising-like model, the system is expected to show a first-order transition, while a gradual conversion is obtained in the simulations. However, for the lattice  $4 \times 4$ , we obtained a first-order transition with a hysteresis at  $T_{eq} \sim 186$  K, which satisfies the usual criteria of occurrence of first-order transitions in Ising-like model. Figure 6 showing the behavior of the thermal hysteresis width *versus* the system sizes summarizes the results. The system undergoes a gradual SCO transition for sizes larger than  $N_x = 6$ , and shows first order transitions below this critical value. Interestingly,  $N_x = 6$  corresponds to the value at which we observe between the number of particles in the bulk  $(N_x - 2)^2$  and that at the surface,  $4(N_x - 1)$ . This fact demonstrates that the surface is playing the major role in driving the spin transition in this problem, as observed in experiments. The competition between the core and surface molecules are driven by the long-range,  $G$ , and the surface,  $L$ , interactions, and then the critical size to obtain the first-order transition is a function of the rate of these interaction parameters.

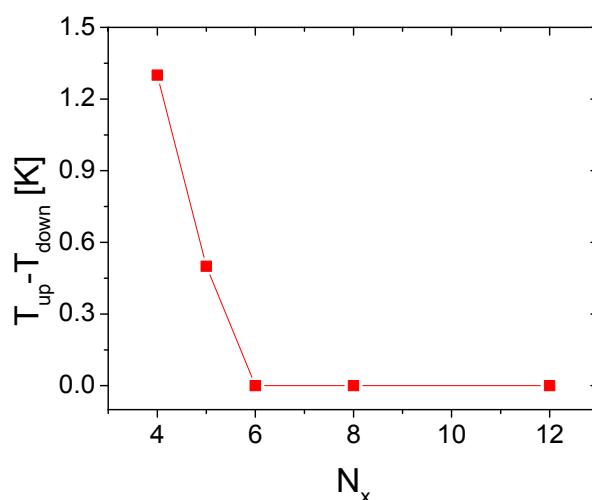


**Figure 6.** Size dependence of the thermal hysteresis width showing a drop of the bistability for nanoparticle larger than  $6 \times 6$ . The model parameters are the same as those of Figure 1.

## 5. Conclusions

The impact of specific conditions at the edges of SCO nanoparticles have been investigated in a 2-D model in which a smaller ligand field was affected to surface atoms, based on the experimental observation of a decreasing transition temperature and an increasing thermal hysteresis width upon particle size reduction. This specific boundary condition basically acts as a negative pressure, shifting downwards the equilibrium temperature, however, in a size-dependent way. The interplay between this equilibrium temperature variation and the expected Curie temperature, arising from a pure Ising model, explains the enhancement of the width of the thermal hysteresis loop upon size reduction.

Further aspects related to the nanoparticle problem remain to be explored: the existence of a re-entrant first-order spin transition on decreasing the particle size will be analyzed using the same ideas developed throughout the manuscript.

**Acknowledgments:** The present work has been supported by the French “Ministère de la Recherche”, University of Versailles, CNRS and ANR BISTA-MAT: ANR-12-BS07-0030-01, whose support is highly appreciated. CHAIR Materials Simulation and Engineering, UVSQ, Université Paris Saclay is gratefully acknowledged. The Romanian national authority for scientific research, CNCS-UEFISCDI (PN-II-RU-TE-2014-4-2695) is also acknowledged.

**Author Contributions:** J.L. and K.B. have conceived the model and the physical idea, C.M.J. and J.L. has make the numerical calculations, J.L., K.B. and C.M.J. have wrote the paper and participated to all the discussions.

**Conflicts of Interest:** The authors declare no conflict of interest.

## Abbreviations

The following abbreviations are used in this manuscript:

ANR	Agence Nationale de la Recherche
BISTA-MAT	Bistabilité Magnétique
CNRS	Centre national de la recherche scientifique
GEMAC	Groupe d'Etudes de la Matière Condensée
LISV	Laboratoire d'Ingénierie des Systèmes de Versailles
MECS	Monte Carlo Entropic Sampling
SCO	Spin Crossover
UVSQ	Université de Versailles Saint Quentin en Yvelines

## References

- Gutlich, P. Spin crossover in iron(II)-complexes. *Struct. Bond.* **1981**, *44*, 83–195.
- Kahn, O.; Launay, J.P. Molecular bistability: An overview. *Chemtronics* **1988**, *3*, 140–151.
- Jeftic, J.; Hauser, A. Pressure study of the thermal spin transition and the high-spin->low-spin relaxation in the  $R3^-$  and  $P1^-$  crystallographic phases of  $[Zn_{1-x}Fe_x(ptz)_6](BF_4)_2$  single crystals ( $x = 0.1, 0.23$ , and  $1$ ;  $ptz = 1-n$ -propyltetrazole). *J. Phys. Chem. B* **1997**, *101*, 10262–10270. [[CrossRef](#)]
- Molnar, G.; Niel, V.; Real, J.A.; Dubrovinsky, L.; Bousseksou, A.; McGarvey, J.J. Raman spectroscopic study of pressure effects on the spin-crossover coordination polymers  $Fe(Pyrazine)[M(CN)_4] \cdot 2H_2O$  ( $M = Ni, Pd, Pt$ ). First observation of a piezo-hysteresis loop at room temperature. *J. Phys. Chem. B* **2003**, *107*, 3149–3155. [[CrossRef](#)]
- Decurtins, S.; Gutlich, P.; Kohler, C.P.; Spiering, H.; Hauser, A. Light-induced excited spin state trapping in a transition-metal complex: The hexa-1-propyltetrazole-iron (II) tetrafluoroborate spin-crossover system. *Chem. Phys. Lett.* **1984**, *105*, 1–4. [[CrossRef](#)]
- Gütlich, P.; Hauser, A.; Spiering, H. Thermal and optical switching of iron (II) complexes. *Angew. Chem. Int. Edit.* **1994**, *33*, 2024–2054. [[CrossRef](#)]
- Bonhommeau, S.; Molnar, G.; Galet, A.; Zwick, A.; Real, J.A.; McGarvey, J.J.; Bousseksou, A. One shot laser pulse induced reversible spin transition in the spin-crossover complex  $[Fe(C_4H_4N_2)]\{Pt(CN)_4\}$  at room temperature. *Angew. Chem. Int. Edit.* **2005**, *44*, 4069–4073. [[CrossRef](#)] [[PubMed](#)]
- Moussa, N.O.; Molnar, G.; Bonhommeau, S.; Zwick, A.; Mouri, S.; Tanaka, K.; Real, J.A.; Bousseksou, A. Selective photoswitching of the binuclear spin crossover compound  $\{[Fe(bt)(NCS)_2]_2(bpm)\}$  into two distinct macroscopic phases. *Phys. Rev. Lett.* **2005**, *94*. [[CrossRef](#)] [[PubMed](#)]
- Decurtins, S.; Gutlich, P.; Hasselbach, K.M.; Hauser, A.; Spiering, H. Light-induced excited-spin-state trapping in iron (II) spin-crossover systems—Optical spectroscopic and magnetic-susceptibility study. *Inorg. Chem.* **1985**, *24*, 2174–2178. [[CrossRef](#)]
- Bousseksou, A.; Boukheddaden, K.; Goiran, M.; Consejo, C.; Boillot, M.L.; Tuchagues, J.P. Dynamic response of the spin-crossover solid  $Co(H_2(fsa)_2en)(py)_2$  to a pulsed magnetic field. *Phys. Rev. B* **2002**, *65*. [[CrossRef](#)]
- König, E. Nature and dynamics of the spin-state interconversion in metal-complexes. *Struct. Bond.* **1991**, *76*, 51–152.
- Kahn, O. Spin-crossover molecular materials. *Curr. Opin. Solid State Mater. Sci.* **1996**, *1*, 547–554. [[CrossRef](#)]
- Krober, J.; Codjovi, E.; Kahn, O.; Groliere, F.; Jay, C. A spin transition system with a thermal hysteresis at room-temperature. *J. Am. Chem. Soc.* **1993**, *115*, 9810–9811. [[CrossRef](#)]
- Gallois, B.; Real, J.A.; Hauw, C.; Zarembowitch, J. Structural changes associated with the spin transition in bis(isothiocyanato)bis(1,10-phenanthroline)iron: A single-crystal x-ray investigation. *Inorg. Chem.* **1990**, *29*, 1152–1158. [[CrossRef](#)]
- Müller, E.W.; Enslin, J.; Spiering, H.; Gütlich, P. High-spin  $\rightleftharpoons$  low-spin transition in hexacoordinate complexes of iron (II) with monodentate 1-alkyltetrazole ligands: A variable-temperature moessbauer, magnetic susceptibility, and far-infrared study. *Inorg. Chem.* **1983**, *22*, 2074–2078. [[CrossRef](#)]

16. Vos, G.; Le Febre, R.A.; De Graaff, R.A.G.; Haasnoot, J.G.; Reedijk, J. Unique high-spin-low-spin transition of the central ion in a linear, trinuclear iron (II) triazole compound. *J. Am. Chem. Soc.* **1983**, *105*, 1682–1683. [[CrossRef](#)]
17. König, E.; Ritter, G.; Kulshreshtha, S.K.; Waigel, J.; Goodwin, H.A. The discontinuous high-spin (5T<sub>2</sub>)⇌low-spin (1A<sub>1</sub>) transition in solid bis(1,10-phenanthroline-2-carbaldehyde phenylhydrazone)iron(II) bis(tetrafluoroborate): Hysteresis effects, concurrent crystallographic phase change, entropy of the transition, and effect of pressure. *Inorg. Chem.* **1984**, *23*, 1896–1902.
18. König, E.; Ritter, G.; Grunsteudel, H.; Dengler, J.; Nelson, J. Effect of a simultaneous change of temperature and pressure on the spin-state transition in bis(thiocyanato)bis(2,2'-bi-2-thiazoline)iron(II). *Inorg. Chem.* **1994**, *33*, 837–839. [[CrossRef](#)]
19. Ksenofontov, V.; Spiering, H.; Schreiner, A.; Levchenko, G.; Goodwin, H.A.; Gutlich, P. The influence of hydrostatic pressure on hysteresis phase transition in spin crossover compounds. *J. Phys. Chem. Solids* **1999**, *60*, 393–399. [[CrossRef](#)]
20. Bousseksou, A.; Molnar, G.; Demont, P.; Menegotto, J. Observation of a thermal hysteresis loop in the dielectric constant of spin crossover complexes: Towards molecular memory devices. *J. Mater. Chem.* **2003**, *13*, 2069–2071. [[CrossRef](#)]
21. Morscheidt, W.; Jeftic, J.; Codjovi, E.; Linares, J.; Bousseksou, A.; Constant-Machado, H.; Varret, F. Optical detection of the spin transition by reflectivity: Application to [Fe<sub>x</sub>Co<sub>1-x</sub>(btr)<sub>2</sub>(NCS)<sub>2</sub>]·H<sub>2</sub>O. *Meas. Sci. Technol.* **1998**, *9*, 1311–1315. [[CrossRef](#)]
22. Kahn, O. *Molecular Magnetism*; VCH: New York, NY, USA, 1993.
23. Kahn, O.; Krober, J.; Jay, C. Spin transition molecular materials for displays and data recording. *Adv. Mater.* **1992**, *4*, 718–728. [[CrossRef](#)]
24. Coronado, E.; Galan-Mascaros, J.R.; Monrabal-Capilla, M.; Garcia-Martinez, J.; Pardo-Ibanez, P. Bistable spin-crossover nanoparticles showing magnetic thermal hysteresis near room temperature. *Adv. Mater.* **2007**, *19*, 1359–1361. [[CrossRef](#)]
25. Forestier, T.; Mornet, S.; Daro, N.; Nishihara, T.; Mouri, S.; Tanaka, K.; Fouche, O.; Freysz, E.; Letard, J.F. Nanoparticles of iron(II) spin-crossover. *Chem. Commun.* **2008**, 4327–4329. [[CrossRef](#)] [[PubMed](#)]
26. Volatron, F.; Catala, L.; Riviere, E.; Gloter, A.; Stephan, O.; Mallah, T. Spin-crossover coordination nanoparticles. *Inorg. Chem.* **2008**, *47*, 6584–6586. [[CrossRef](#)] [[PubMed](#)]
27. Boldog, I.; Gaspar, A.B.; Martínez, V.; Pardo-Ibañez, P.; Ksenofontov, V.; Bhattacharjee, A.; Gütllich, P.; Real, J.A. Spin-crossover nanocrystals with magnetic, optical, and structural bistability near room temperature. *Angew. Chem.* **2008**, *120*, 6533–6537. [[CrossRef](#)]
28. Forestier, T.; Kaiba, A.; Pechev, S.; Denux, D.; Guionneau, P.; Etrillard, C.; Daro, N.; Freysz, E.; Letard, J.F. Nanoparticles of [Fe(NH<sub>2</sub>-trz)<sub>3</sub>]Br<sub>2</sub>·3H<sub>2</sub>O (NH<sub>2</sub>-trz = 2-Amino-1,2,4-triazole) prepared by the reverse micelle technique: Influence of particle and coherent domain sizes on spin-crossover properties. *Chem. Eur. J.* **2009**, *15*, 6122–6130. [[CrossRef](#)] [[PubMed](#)]
29. Catala, L.; Volatron, F.; Brinzei, D.; Mallah, T. Functional coordination nanoparticles. *Inorg. Chem.* **2009**, *48*, 3360–3370. [[CrossRef](#)] [[PubMed](#)]
30. Galan-Mascaros, J.R.; Coronado, E.; Forment-Aliaga, A.; Monrabal-Capilla, M.; Pinilla-Cienfuegos, E.; Ceolin, M. Tuning size and thermal hysteresis in bistable spin crossover nanoparticles. *Inorg. Chem.* **2010**, *49*, 5706–5714. [[CrossRef](#)] [[PubMed](#)]
31. Thibault, C.; Molnar, G.; Salmon, L.; Bousseksou, A.; Vieu, C. Soft lithographic patterning of spin crossover nanoparticles. *Langmuir* **2010**, *26*, 1557–1560. [[CrossRef](#)] [[PubMed](#)]
32. Martínez, V.; Boldog, I.; Gaspar, A.B.; Ksenofontov, V.; Bhattacharjee, A.; Gütllich, P.; Real, J.A. Spin crossover phenomenon in nanocrystals and nanoparticles of [Fe(3-Fpy)<sub>2</sub>M(CN)<sub>4</sub>] (MII = Ni, Pd, Pt) two-dimensional coordination polymers. *Chem. Mater.* **2010**, *22*, 4271–4281. [[CrossRef](#)]
33. Tissot, A.; Bardeau, J.-F.; Riviere, E.; Brisset, F.; Boillot, M.-L. Thermo- and photoswitchable spin-crossover nanoparticles of an iron(II) complex trapped in transparent silica thin films. *Dalton Trans.* **2010**, *39*, 7806–7812. [[CrossRef](#)] [[PubMed](#)]
34. Rotaru, A.; Varret, F.; Gindulescu, A.; Linares, J.; Stancu, A.; Letard, J.; Forestier, T.; Etrillard, C. Size effect in spin-crossover systems investigated by force measurements, for surfacted [Fe(NH<sub>2</sub>-trz)<sub>3</sub>](Br)<sub>2</sub>·3H<sub>2</sub>O nanoparticles: Reversible contributions and critical size. *Eur. Phys. J. B* **2011**, *84*, 439–449. [[CrossRef](#)]

35. Jetic, J.; Menendez, N.; Wack, A.; Coddjovi, E.; Linares, J.; Goujon, A.; Hamel, G.; Klotz, S.; Syfosse, G.; Varret, F. A helium-gas-pressure apparatus with optical-reflectivity detection tested with a spin-transition solid. *Meas. Sci. Technol.* **1999**, *10*, 1059–1064. [[CrossRef](#)]
36. Kawamoto, T.; Abe, S. Thermal hysteresis loop of the spin-state in nanoparticles of transition metal complexes: Monte carlo simulations on an ising-like model. *Chem. Commun.* **2005**, 3933–3935. [[CrossRef](#)] [[PubMed](#)]
37. Nicolazzi, W.; Pillet, S.; Lecomte, C. Two-variable anharmonic model for spin-crossover solids: A like-spin domains interpretation. *Phys. Rev. B* **2008**, *78*. [[CrossRef](#)]
38. Konishi, Y.; Tokoro, H.; Nishino, M.; Miyashita, S. Monte carlo simulation of pressure-induced phase transitions in spin-crossover materials. *Phys. Rev. Lett.* **2008**, *100*. [[CrossRef](#)] [[PubMed](#)]
39. Enachescu, C.; Constant-Machado, H.; Coddjovi, E.; Linares, J.; Boukheddaden, K.; Varret, F. Direct access to the photo-excitation and relaxation terms in photo-switchable solids: Non-linear aspects. *J. Phys. Chem. Solids* **2001**, *62*, 1409–1422. [[CrossRef](#)]
40. Wajnflasz, J.; Pick, R. Transitions " low spin " - " high spin " dans les complexes de  $Fe^{2+}$ . *J. Phys. Colloques* **1971**, *32*, 91–92. [[CrossRef](#)]
41. Bousseksou, A.; Nasser, J.; Linares, J.; Boukheddaden, K.; Varret, F. Ising-like model for the 2-step spin-crossover. *J. De Phys. I* **1992**, *2*, 1381–1403. [[CrossRef](#)]
42. Boukheddaden, K.; Shteto, I.; Hoo, B.; Varret, F. Dynamical model for spin-crossover solids. I. Relaxation effects in the mean-field approach. *Phys. Rev. B* **2000**, *62*, 14796–14805. [[CrossRef](#)]
43. Linares, J.; Spiering, H.; Varret, F. Analytical solution of 1d ising-like systems modified by weak long range interaction - application to spin crossover compounds. *Eur. Phys. J. B* **1999**, *10*, 271–275. [[CrossRef](#)]
44. Chiruta, D.; Jureschi, C.-M.; Linares, J.; Dahoo, P.; Garcia, Y.; Rotaru, A. On the origin of multi-step spin transition behaviour in 1d nanoparticles. *Eur. Phys. J. B* **2015**, *88*, 1–5. [[CrossRef](#)]
45. Shteto, I.; Linares, J.; Varret, F. Monte carlo entropic sampling for the study of metastable states and relaxation paths. *Phys. Rev. E* **1997**, *56*, 5128–5137. [[CrossRef](#)]
46. Linares, J.; Enachescu, C.; Boukheddaden, K.; Varret, F. Monte carlo entropic sampling applied to spin crossover solids: The squareness of the thermal hysteresis loop. *Polyhedron* **2003**, *22*, 2453–2456. [[CrossRef](#)]
47. Linares, J.; Jureschi, C.-M.; Boulmaali, A.; Boukheddaden, K. Matrix and size effects on the appearance of the thermal hysteresis in 2d spin crossover nanoparticles. *Phys. B Condens. Matter.* **2016**, *486*, 164–168. [[CrossRef](#)]
48. Muraoka, A.; Boukheddaden, K.; Linares, J.; Varret, F. Two-dimensional ising-like model with specific edge effects for spin-crossover nanoparticles: A monte carlo study. *Phys. Rev. B* **2011**, *84*. [[CrossRef](#)]



© 2016 by the authors; licensee MDPI, Basel, Switzerland. This article is an open access article distributed under the terms and conditions of the Creative Commons Attribution (CC-BY) license (<http://creativecommons.org/licenses/by/4.0/>).